Intersystem-crossing and excited-state absorption of C_{70} studied by picosecond pump and probe absorption and fluorescence measurements

S. Reindl, A. Penzkofer *, H. Gratz

Institut II—Experimentelle und Angewandte Physik, Universität Regensburg, D-93040 Regensburg, Germany

Abstract

The singlet and triplet absorption and emission dynamics of C_{70} in toluene is studied with a picosecond Nd:glass laser double-pulse pump and probe transmission and fluorescence measurement technique. The singlet S_1 excited-state absorption ($\sigma_{ex,L} \approx 6 \times 10^{-17}$ cm^2), the triplet T_1 absorption ($\sigma_T \approx 4.2 \times 10^{-17}$ cm^2), and the triplet T_2 absorption ($\sigma_{ex,T} \approx 4.3 \times 10^{-17}$ cm^2) at 527 nm are determined. The singlet to triplet intersystem-crossing is studied by double pump pulse induced fluorescence signal analysis and by double probe pulse transmission measurements. The yield of triplet formation is found to be near to unity.   © 1998 Elsevier Science S.A. All rights reserved.

1. Introduction

Since the discovery [1] and laboratory synthesis [2] of fullerenes their study is an active field of research [3]. The optical spectroscopy of C_{60} and C_{70} is reviewed in Refs. [3,4]. The ground-state absorption of C_{60} [4–8] and C_{70} [4,6–8] was analysed. Fluorescence studies of C_{60} [9–12] and C_{70} [9,11–15] have been performed. Small quantum yields of fluorescence ($\phi_F \approx 2.2 \times 10^{-4}$ for C_{60} [10], and $\phi_F = 5.9 \times 10^{-4}$ [14] to 8.5×10^{-4} [9,16] for C_{70}) were determined. The yield of triplet formation was found to be close to 100% (C_{60}: [4,17]; C_{70}: [4,18–21]). Triplet–triplet absorption spectra for C_{60} and C_{70} are presented in Refs. [4,19,20,22,23] and Refs. [4,20,21,23,24], respectively.

The excited-state absorption of C_{60} [11,25–33] [34–40] and C_{70} [11,15,24,26–28] has been studied mainly with respect to optical limiting applications (reverse saturable absorption) [28–32,34,35,38–41].

In this paper the singlet and triplet absorption and emission dynamics of C_{70} in toluene at room temperature is investigated. The S_1–S_n ($n > 2$) singlet–singlet, the T_1–T_l ($l \geq 2$) and the T_2–T_m ($m \geq 3$) triplet– triplet absorption cross-sections at 527 nm, and the quantum yield of triplet formation by S_1–T_1 intersystem-crossing (population accumulation in T_1 state after intersystem-crossing) are determined.

Picosecond second-harmonic pulses of a mode-locked Nd:glass laser are used in the experiments. A double pump-pulse and double probe-pulse transmission [42] and a double pump pulse induced fluorescence measurement technique [43,44] are applied. Some absorption cross-sections and the quantum yield of triplet formation are deduced by comparing the experimental results with numerical simulations of the absorption and emission dynamics. The first picosecond pump pulse transmission depends on the S_1–S_n excited-state absorption dynamics (excited-state absorption cross-section, $\sigma_{ex,L}$, and S_n-state relaxation time, τ_{ex}). The first probe pulse transmission is caused by the residual S_0-ground-state absorption and the induced T_1–T_1 triplet–triplet absorption at the time, t_D, of probe pulse passing. It depends on the yield of triplet formation, ϕ_T, and the T_1 triplet absorption cross-section, σ_T. The second pump pulse transmission depends on the singlet–singlet and triplet–triplet absorption and relaxation dynamics. It allows to extract the higher excited-state T_2–T_m absorption cross-section, $\sigma_{ex,T}$. The second probe pulse transmission depends on the population accumulation in the T_1 triplet state. The second probe pulse transmission together with the first probe pulse transmission allows the separate determination of σ_T and ϕ_T.

The first pump pulse induced fluorescence signal, $S_{F,1}$, is determined by the pump pulse induced S_1-state level population and the fluorescence quantum yield. The second pump pulse induced fluorescence signal, $S_{F,2}$, is reduced compared to the first pump pulse induced fluorescence signal in the case

* Corresponding author. E-mail: alfons.penzkofer@physik.uni-regensburg.de

of singlet–triplet intersystem-crossing since then the S_1-state level population is reduced. The ratio of $S_{F,2}/S_{F,1}$ allows the determination of the quantum yield of triplet formation, ϕ_T [43,44].

The S_1–S_n excited-state absorption cross-section, $\sigma_{ex,L}$, and the T_1–T_i absorption cross-section are found to be larger than the S_0 ground-state absorption cross-section, σ_L (reverse saturable absorption [40]). The quantum yield of triplet formation, σ_T, by S_1–T_1 intersystem-crossing is determined to be close to 100%.

2. Experimental

The fullerene C_{70} was purchased from Aldrich ([5,6]-Fullerene C_{70}) and is used without further purification. The solvent toluene is of analytical grade. The absorption cross-section spectrum, $\sigma_a(\lambda)$, of C_{70} in toluene at room temperature is displayed in Fig. 1 together with the fluorescence quantum distribution $E_F(\lambda)$ (own measurements).

The double-pulse pump and probe transmission measurements have been carried out with a picosecond Nd:glass laser system [45]. The experimental arrangement is displayed in Fig. 2. The mode-locked laser generates a train of picosecond pulses. The time period of adjacent pulses is $t_R = 10$ ns (resonator roundtrip time). Two adjacent pulses are separated from the pulse train by an electro-optic switch [47] and increased in energy by a Nd:phosphate glass laser amplifier. The pulses are frequency doubled in a CDA crystal [48] and the remaining fundamental light is filtered off (filter F1). The wavelength of the second-harmonic pump pulses is $\lambda_L = 527$ nm. The pump pulse duration is $\Delta t_L = 6$ ps. The second harmonic pump pulses are directed to the sample, S (cell thickness $l = 1$ mm). They are increased in intensity by lens L1. The input peak energy density is determined by energy transmission measurement through rhodamine 6G in ethanol (saturable absorption [46]) with photodetectors PD1 and PD2. The energy transmission of the pump pulses is measured with the photodetectors PD1 and PD3 (small signal transmission $T_0 = 0.0756 \pm 0.001$). The probe pulses are split-off from the pump pulses with a beam splitter and are attenuated with a filter (F2). They pass opposite to the pump pulse direction through the sample. Their temporal delay relative to the pump pulses is $t_D = 9$ ns. The probe pulse diameter is adjusted by lens L2. The transmission of the probe pulses is registered with the detectors the PD1 and PD4.

The double-pump-pulse fluorescence measurements are carried out with the probe beam path covered. The fluorescence emitted in sideward direction is collected with lens, L3, and directed to the spectrometer, SP, with lens, L4. The fluorescence light in the spectral region from 640 to 840 nm is passed through the spectrometer and registered temporally resolved with a microchannel-plate photomultiplier (Hamamatsu type R1564U) and a fast digital oscilloscope (LeCroy type 9362, time resolution approximately 500 ps).
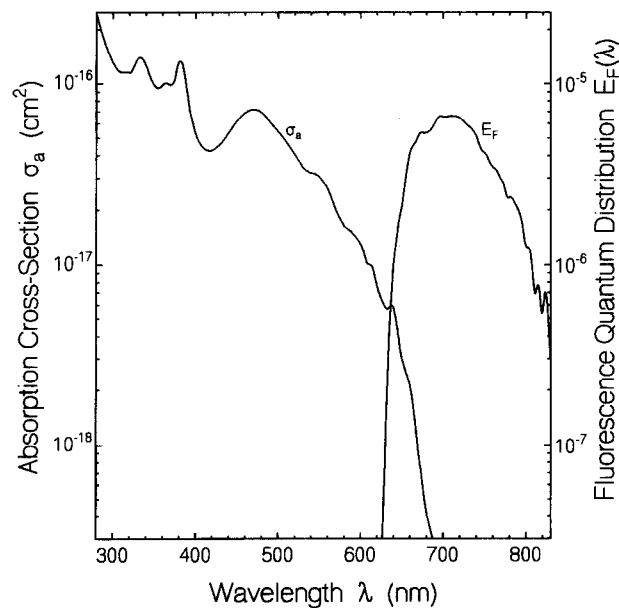

Fig. 1. Absorption cross-section spectrum, $\sigma_a(\lambda)$, and fluorescence quantum distribution, $E_F(\lambda)$, of C_{70} dissolved in toluene.
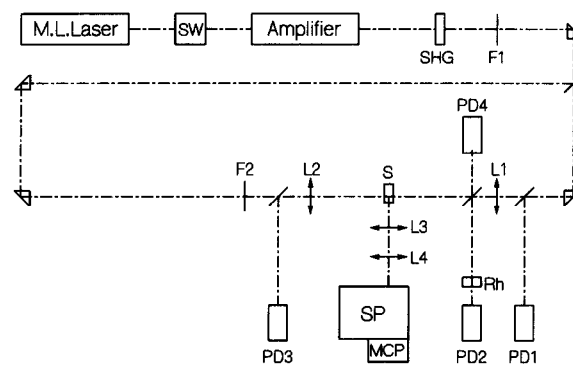

Fig. 2. Experimental setup. M.L. Laser, mode-locked Nd:glass laser. SW, single pulse selector. Amplifier, Nd:glass laser amplifier. SHG, frequency doubler. F1, cut-off filter of fundamental laser wavelength. L1–L4, lenses. Rh, rhodamine 6G in ethanol for energy density measurement [46]. PD1–PD4, photodetectors. S, sample. SP, spectrometer. MCP, microchannel-plate photomultiplier.

The intensity dependent transmission behaviour of the solvent toluene was measured separately with the experimental arrangement of Fig. 2 (pure toluene in sample cell, S). The measured energy transmission vs. input pump pulse peak intensity is displayed in Fig. 3. The transmission reduction at high pump pulse intensities is thought to be due to two-photon absorption [49]. The curves in Fig. 3 are calculated for various two-photon absorption coefficients, $\alpha^{(2)}$. The best fit is obtained for $\alpha^{(2)} = (2 \pm 0.3) \times 10^{-10}$ cm/W. The two-photon absorption of the solvent is included in the analysis of the experimental results.

3. Experimental results

The pump pulse energy transmissions, $T_{E,L1}$, $T_{E,L2}$, the probe pulse energy transmissions, T_{P1}, T_{P2}, and the pump
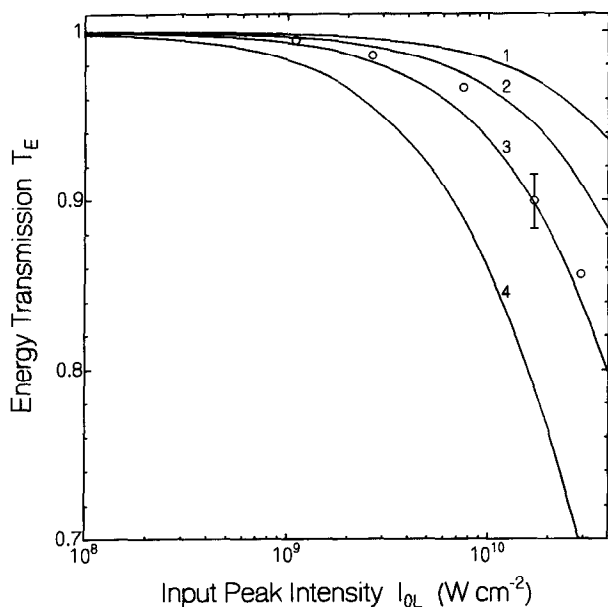
Fig. 3. Energy transmission through toluene. Pump laser wavelength, $\lambda_L = 527$ nm. Sample length $l = 1$ mm. Circles, experimental points. Curves are calculated for $\alpha^{(2)} = 5 \times 10^{-11}$ cm/W (1), 1×10^{-10} cm/W (2), 2×10^{-10} cm/W (3), and 5×10^{-10} cm/W (4).

Fig. 4. Energy transmission, $T_{E,L1}$, of first pump pulse through C_{70} in toluene vs. input pump pulse peak intensity, $I_{0L,1}$. Small signal transmission, $T_0 = 0.0756$. Circles are experimental data points. Curves are calculated using parameters of Table 1. Solid curves, $\tau_{ex} = 60$ fs with $\sigma_{ex,L} = 4 \times 10^{-17}$ cm^2 (1), 5×10^{-17} cm^2 (2), 6×10^{-17} cm^2 (3), 7×10^{-17} cm^2 (4). Dashed curves, $\sigma_{ex,L} = 6 \times 10^{-17}$ cm^2 with $\tau_{ex} = 300$ fs (a), 200 fs (b), 100 fs (c).

pulse induced fluorescence signal heights, $S_{F,1}$, $S_{F,2}$, are measured as a function of the first pump pulse input peak intensity, $I_{0L,1}$. Data are selected where the second pump pulse peak intensity, $I_{0L,2}$, is approximately equal to the first pump pulse peak intensity. The probe pulse peak intensities are kept a factor of 250 smaller than the pump pulse peak intensities. The probe beam diameters were a factor of two narrower than the pump beam diameters at the sample position. The saturation intensity of S_0 ground-state depopulation, $I_{sat} = h\nu_L / (\sigma_L \Delta t_L)$ (h, Planck constant; ν_L, second harmonic laser frequency; σ_L absorption cross-section at ν_L; Δt_L, duration of second harmonic pulses), is marked in Figs. (4)–(8) (slow saturable absorption conditions apply since $\Delta t_L \ll \tau_{S_1}$, where τ_{S_1} is the S_1-state lifetime [50]).

The energy transmission, $T_{E,L1}$, of the first pump pulse ($\lambda_L = 527$ nm, $\Delta t_L = 6$ ps) through C_{70} in toluene (small signal transmission $T_0 = 0.0756$) is displayed by circles in Fig. 4. The transmission decreases with rising input pump pulse intensity. The behaviour indicates that the excited-state absorption is larger than the ground-state absorption at 527 nm (reverse saturable absorption).

The energy transmission, $T_{E,L2}$, of the second pump pulse (time delay $t_R = 10$ ns) through the sample is shown by circles in Fig. 5. The decrease in transmission with rising pump pulse intensity is similar to the behaviour of the first pulse. It indicates a larger T_1-triplet absorption than S_0-singlet absorption.

The first probe pulse transmission, T_{P1} (time delay $t_D = 9$ ns) is displayed by circles in Fig. 6. Its dependence is determined by the S_0 ground-state absorption of the molecules, which have remained in the S_0-state, and by the T_1-triplet absorption of the molecules, which have proceeded to
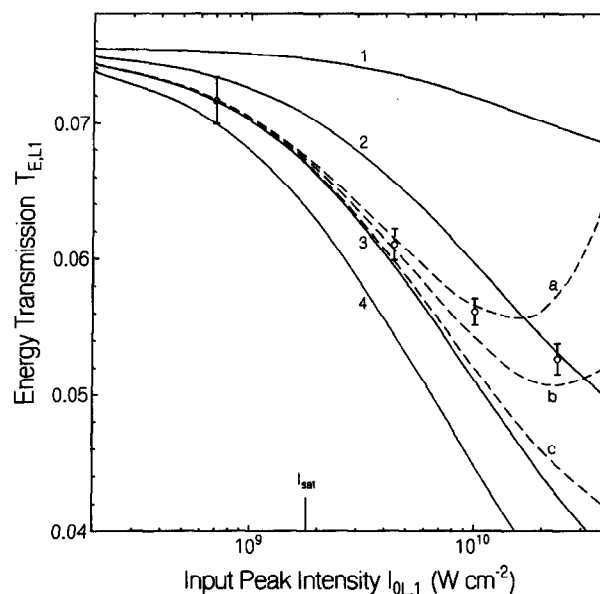

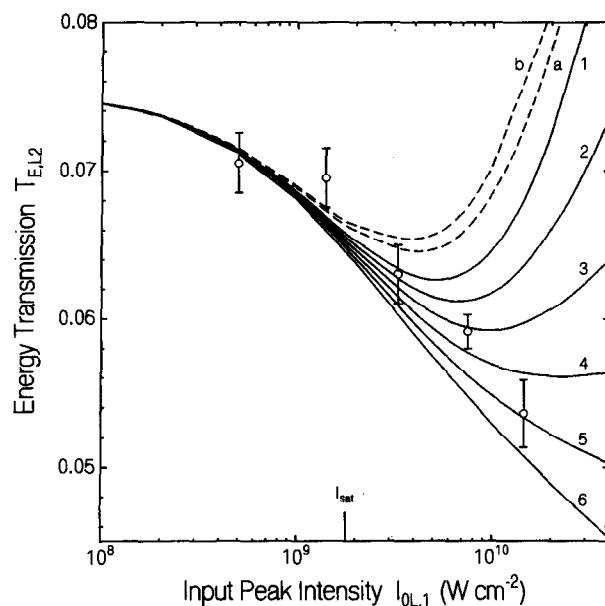Fig. 5. Energy transmission of second pump pulse, $T_{E,L2}$, vs. input peak intensity of first pump pulse (second pump pulse peak intensity is nearly the same as first pump pulse peak intensity). Circles are experimental data points. All curves are calculated for $\sigma_T = 4.2 \times 10^{-17}$ cm^2. Solid curves, $\tau_T = 2$ ps and $\sigma_{ex,T} = 2.5 \times 10^{-17}$ cm^2 (1), 3×10^{-17} cm^2 (2), 3.5×10^{-17} cm^2 (3), 4×10^{-17} cm^2 (4), 4.5×10^{-17} cm^2 (5), and 5×10^{-17} cm^2 (6). Dashed curves, $\sigma_{ex,T} = 2.5 \times 10^{-17}$ cm^2 and $\tau_T = 10$ ps (a), 100 ps (b). Other parameters are taken from Table 1.

the T_1-state. The probe pulse transmission reduces with rising first pump pulse peak intensity, $I_{0L,1}$. But the decrease in transmission of the first probe pulse is slightly smaller than the decrease of transmission of the first pump pulse indicating
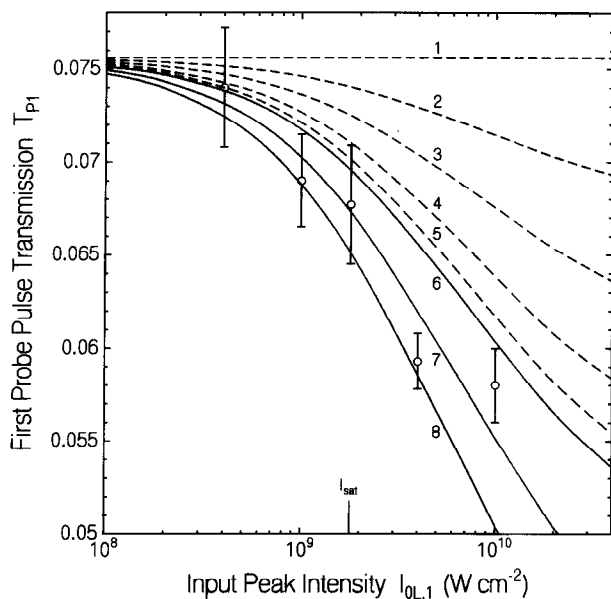
Fig. 6. Transmission of first probe pulse, T_{P1}, vs. first pump pulse peak intensity, $I_{0L,1}$. Circles are experimental results. The curves are calculated using the parameters of Table 1. Dashed curves, $\sigma_T = 4 \times 10^{-17}$ cm^2 and $\phi_T = 0$ (1), 0.25 (2), 0.5 (3), 0,75 (4), and 0.9 (5). Solid curves, $\phi_T = 0.999$ and $\sigma_T = 4 \times 10^{-17}$ cm^2 (6), 4.2×10^{-17} cm^2 (7), and 4.4×10^{-17} cm^2 (8).

Fig. 8. Fluorescence signal ratio, $S_{F,2}/S_{F,1}$, vs. input peak intensity, $I_{0L,1}$. Circles are experimental data. $T_0 = 0.0756$. Differences in peak intensity of first and second pump pulse are corrected by $S_{F,2}/S_{F,1} = (S_{F,2}/S_{F,1})_{measured}$ $[I_{0L,1}/(1 + I_{0L,1}/I_{sat})]/[I_{0L,2}/(1 + I_{0L,2}/I_{sat})]$. The curves are calculated for parameters of Table 1 and $\phi_T = 0$ (1), 0.25 (2), 0.5 (3), 0.75 (4), 0.9 (5), and 0.999 (6).

The fluorescence signal ratio, $S_{F,2}/S_{F,1}$, of the second pump pulse induced peak fluorescence signal height to the first pump pulse induced peak fluorescence signal height is displayed in Fig. 8 (circles) as a function of the first pump pulse peak intensity, $I_{0L,1}$. The ratio decreases with increasing $I_{0L,1}$ indicating triplet level population by intersystem-crossing.

4. Theoretical description

An extraction of the absorption cross-sections, $\sigma_{ex,L}$, σ_T, $\sigma_{ex,T}$, of the higher-excited-singlet-state relaxation time, τ_{ex}, and of the S_1–T_1 intersystem-crossing rate, k_{35}, from the experimental transmission and fluorescence data requires a theoretical description of the absorption and emission dynamics and a numerical simulation of the experimental results.

The absorption dynamics of the two pump pulses and the two probe pulses is analysed using the energy level system of Fig. 9a and the double pump pulse and double probe pulse scheme of Fig. 9b. All pulses are linearly polarized in the same direction. The pump pulse induced fluorescence dynamics is determined by the dynamics of the S_1-level population.

4.1. Level population and pulse propagation model

The first pump pulse excites molecules from the S_0-ground-state (level 1) to an excited singlet state (level 2; ground-state absorption cross-section, σ_L). From there the molecules relax quickly (Franck–Condon relaxation time constant, $\tau_{FC,S}$) to a thermal equilibrium position in the S_1-band (level
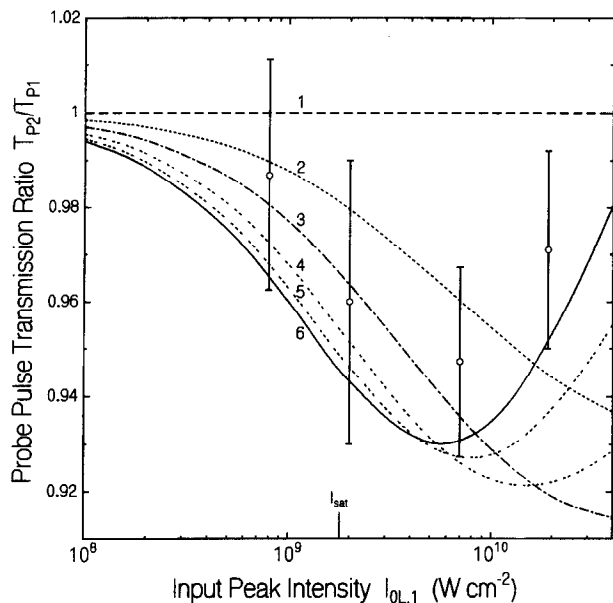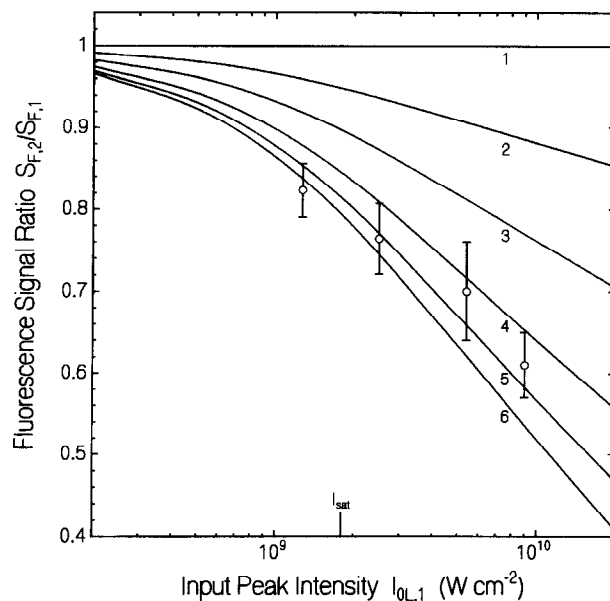

Fig. 7. Transmission ratio of probe pulses T_{P2}/T_{P1}, vs. input peak intensity of first pump pulse, $I_{0L,1}$. Circles are experimental data. Error bars show standard deviation of the mean transmission ratios. The curves are calculated for $\phi_T = 0$ (1), 0.25 (2), 0.5 (3), 0.75 (4), 0.9 (5), 0.999 (6). Other parameters are taken from Table 1.

that the T_1-triplet absorption cross-section, σ_T, is smaller than the S_1-state excited-state absorption cross-section, $\sigma_{ex,L}$.

The ratio of second probe pulse transmission to first probe pulse transmission, T_{P2}/T_{P1}, is shown in Fig. 7. The transmission ratio is slightly less than one with a minimum around $I_{0L,1} \approx 7 \times 10^9$ W/cm^2. The intensity dependent behaviour of T_{P1} and T_{P2}/T_{P1} is used below to extract σ_T and ϕ_T.
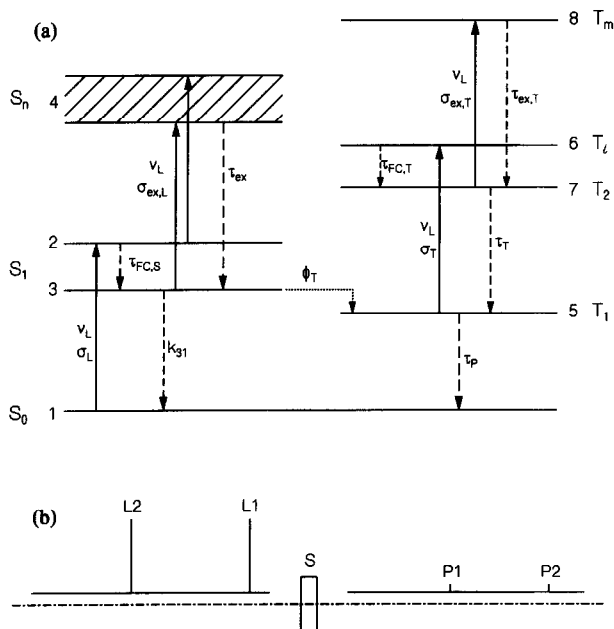
Fig. 9. (a) Energy level scheme for singlet–singlet absorption dynamics, triplet–triplet absorption dynamics, and S_1–T_1 singlet–triplet intersystem-crossing. (b) Scheme of double-pulse pump and double-pulse probe interaction in the sample.

3). From levels 2 and 3 there occurs S_1–S_n excited-state absorption to band 4 (excited-state absorption cross-section, $\sigma_{ex,L}$). The population in level 4 relaxes quickly to level 3 (relaxation time constant, τ_{ex}). The thermally relaxed S_1-state population (level 3) relaxes to the ground-state (relaxation rate constant, k_{31}) and to the triplet system (intersystem-crossing rate constant, k_{35}; yield of triplet formation, ϕ_T). The S_1-state lifetime, τ_{S_1} (equal to the fluorescence lifetime, τ_F) is given by $\tau_{S_1} = (k_{31} + k_{35})^{-1}$. The S_1-state intersystem-crossing rate is $k_{35} = \phi_T \tau_{S_1}^{-1}$.

The first probe pulse, P1, passes through the sample after a time delay of $t_{L1,P1} = t_D$ which is slightly shorter than the temporal pump pulse separation, t_R, but much longer than the S_1-state lifetime, τ_{S_1}. The transmission, T_{P1}, of the probe pulse, P1, is given by the singlet ground-state absorption, which is determined by the S_0-ground-state population number density, $N_1(t' = t_D)$, and by the T_1-triplet absorption, which is determined by the population number density of the lowest triplet state, $N_5(t' = t_D)$ $(N_5(t' = t_D) = N_0 - N_1(t' = t_D)$, where N_0 is the total molecule number density).

The second pump pulse, L2, causes the same absorption and emission dynamics in the singlet system as the first pump pulse (but the initial ground-state population, $N_1(t' = t_R)$, is smaller) and additionally causes excitation and relaxation in the triplet system. The molecules in the triplet ground-state, T_1 (level 5), are excited to a higher lying triplet state, T_1, (level 6, triplet absorption cross-section, σ_T). From there the molecules relax quickly to the lowest excited triplet state, T_2 (Franck–Condon relaxation time constant, $\tau_{FC,T}$). From the T_2-state (level 7) the molecules relax to the T_1-state with a time constant τ_T. The back transfer from T_1 to S_0 occurs with

the phosphorescence lifetime, τ_P, on a microsecond to millisecond time scale [16,18,20,21,51,52].

The second probe pulse passes through the sample after a time delay of $t_{L1,P2} = t_R + t_D$ relative to the first pump pulse. Its transmission is determined by the S_0 (level 1) and T_1 (level 5) population number densities at the time of passing the sample.

Higher excited-state singlet → triplet intersystem-crossing [53–56] and triplet → singlet intersystem-crossing [42,57–60] are not included in the absorption and emission dynamics, since the transmission and fluorescence behaviour can be fitted reasonably well with the presented model and the error bars of the experimental data allow no further model refinement.

4.2. Equation system

The saturable absorption dynamics of the two pump pulses and the two probe pulses is handled by the following differential equation system for the level population number densities, N_1 to N_7, and the laser pulse intensities, I_{L1}, I_{L2}, I_{P1}, and I_{P2} [44]. Immediate relaxation from level 8 to level 7 is assumed ($\tau_{ex,T} = 0$).

$$\frac{\partial N_1}{\partial t'} = -\sigma_L\left(N_1 - N_2\right)\frac{I_{L1} + I_{L2}}{h\nu_L} + k_{31}N_3 + \frac{N_5}{\tau_P} \tag{1}$$

$$\frac{\partial N_2}{\partial t'} = \sigma_L\left(N_1 - N_2\right)\frac{I_{L1} + I_{L2}}{h\nu_L}$$
$$- \sigma_{ex,L}\left(N_2 - \frac{N_2}{N_2 + N_3}N_4\right)\frac{I_{L1} + I_{L2}}{h\nu_L} - \frac{N_2}{\tau_{FC,S}} \tag{2}$$

$$\frac{\partial N_3}{\partial t'} = \frac{N_2}{\tau_{FC,S}} - \sigma_{ex,L}\left(N_3 - \frac{N_3}{N_2 + N_3}N_4\right)\frac{I_{L1} + I_{L2}}{h\nu_L}$$
$$+ \frac{N_4}{\tau_{ex}} - \frac{N_3}{\tau_{S_1}} \tag{3}$$

$$\frac{\partial N_4}{\partial t'} = \sigma_{ex,L}\left(N_2 + N_3 - N_4\right)\frac{I_{L1} + I_{L2}}{h\nu_L} - \frac{N_4}{\tau_{ex}} \tag{4}$$

$$\frac{\partial N_5}{\partial t'} = \frac{\phi_T}{\tau_{S_1}}N_3 - \sigma_T\left(N_5 - N_6\right)\frac{I_{L1} + I_{L2}}{h\nu_L} + \frac{N_7}{\tau_T} - \frac{N_5}{\tau_P} \tag{5}$$

$$\frac{\partial N_6}{\partial t'} = \sigma_T\left(N_5 - N_6\right)\frac{I_{L1} + I_{L2}}{h\nu_L} - \frac{N_6}{\tau_{FC,T}} \tag{6}$$

$$\frac{\partial N_7}{\partial t'} = \frac{N_6}{\tau_{FC,T}} - \frac{N_7}{\tau_T} \tag{7}$$

$$\frac{\partial I_{Li}}{\partial z'} = -\left[\sigma_L\left(N_1 - N_2\right) + \sigma_{ex,L}\left(N_2 + N_3 - N_4\right)\right.$$
$$\left. + \sigma_T\left(N_5 - N_6\right) + \sigma_{ex,T}\left(N_7 + N_6\right)\right]I_{Li} - \alpha^{(2)}I_{Li}^2 \tag{8}$$

$(i = 1,2)$

$$\frac{\partial I_{Pi}}{\partial z'} = -\left[\sigma_L N_1 + \sigma_T N_5\right] I_{Pi} \qquad (i=1,2) \tag{9}$$

$$T_{E,i} = \frac{\displaystyle\int_0^\infty r \int_{-\infty}^\infty I_i(t',l,r)\,\mathrm{d}t'\mathrm{d}r}{\displaystyle\int_0^\infty r \int_{-\infty}^\infty I_i(t',0,r)\,\mathrm{d}t'\mathrm{d}r} \qquad (i=L1,L2,P1,P2) \tag{10}$$

The transformation $t' = t - nz/c_0$ and $z' = z$ is used, where t is the time, z is the distance along the propagation direction, c_0 is the light velocity in vacuum, and n is the refractive index. l is the sample length. An absorption anisotropy is not considered since C_{70} is nearly spherical symmetric [3].

The initial conditions of the level populations are $N_1(t' = -\infty,z',r) = N_0$ and $N_i(t' = -\infty,z',r) = 0$ for $i = 2,...,7$. N_0 is the total number density of dissolved fullerene molecules. The input pulse intensities are

$$I_{L1}(t',z'=0,r) = I_{0L,1}\exp\left[-\left(\frac{t'}{t_0}\right)^2 - \left(\frac{r}{r_L}\right)^2\right] \tag{11}$$

$$I_{L2}(t',z'=0,r) = I_{0L,2}\exp\left[-\left(\frac{t'-t_R}{t_0}\right)^2 - \left(\frac{r}{r_L}\right)^2\right] \tag{12}$$

$$I_{P1}(t',z'=0,r) = I_{0P,1}\exp\left[-\left(\frac{t'-t_D}{t_0}\right)^2 - \left(\frac{r}{r_P}\right)^2\right] \tag{13}$$

$$I_{P2}(t',z'=0,r) = I_{0P,2}\exp\left[-\left(\frac{t'-t_D-t_R}{t_0}\right)^2 - \left(\frac{r}{r_P}\right)^2\right] \tag{14}$$

r is the radial beam coordinate. r_L and r_P are the $1/e$ beam radii of the pump and the probe pulses, respectively. $t_0 = 2^{-1}[\ln(2)]^{-1/2}\Delta t_L$ is half the $1/e$ temporal pulse width (Δt_L is the FWHM pulse duration).

5. Data analysis

The equation system (1)–(10) is solved numerically using relevant parameters of C_{70} in toluene (see Table 1). Unknown parameters are determined by fitting the calculated energy transmissions of the pump and probe beams and the pump pulse induced fluorescence signals to the experimental values.

In Fig. 4 the first pump pulse energy transmission, $T_{E,L1}$, is simulated. $T_{E,L1}$ depends on the S_1-excited-state absorption cross-section, $\sigma_{ex,L}$, and on the S_n-state relaxation time constant, τ_{ex}. The solid curves are calculated for various $\sigma_{ex,L}$-values ($\tau_{ex} = 60$ fs), while the dashed curves are calculated for different S_n-state relaxation times, τ_{ex} ($\sigma_{ex,L} = 6 \times 10^{-17}$ cm²). The best fit to the experimental data is obtained for $\sigma_{ex,L} = 6 \times 10^{-17}$ cm² and $\tau_{ex} = 240$ fs.

The double pump-pulse induced fluorescence signal behaviour is simulated in Fig. 8. The fluorescence signal ratio, $S_{F,2}/S_{F,1}$, depends on the yield of triplet formation, ϕ_T. $S_{F,2}/$ $S_{F,1}$ is practically independent of the explicit triplet–triplet absorption dynamics (verified by numerical simulation, but not shown in Fig. 8). The curves are calculated for various quantum yields of triplet formation, ϕ_T. A comparison of the calculated curves with the experimental data gives $\phi_T = 0.9 \pm 0.1$. The experimental accuracy and subsequently the accuracy of ϕ_T is limited to 10% because the fluorescence quantum yield, ϕ_F, of C_{70} in toluene is very low ($\phi_F \approx 8.5 \times 10^{-4}$, see Table 1).

The first probe pulse transmission, T_{P1}, is simulated in Fig. 6. T_{P1} depends on the quantum yield of triplet formation, ϕ_T, and on the cross-section, σ_T, of $T_1 \to T_l$ triplet–triplet absorption. Knowing ϕ_T, the fitting of calculated T_{P1} curves to experimental data allows the determination of σ_T. The dashed curves in Fig. 6 belong to various ϕ_T values at a fixed value of $\sigma_T = 4 \times 10^{-17}$ cm². The solid curves are calculated for various σ_T values while the triplet quantum yield is fixed to $\phi_T = 0.999$. The best fit to the experimental data is obtained for $\sigma_T = 4.2 \times 10^{-17}$ cm².

The probe pulse transmission ratio, T_{P2}/T_{P1}, is simulated in Fig. 7. The ratio depends on the yield of triplet formation, ϕ_T, and the absorption cross-section ratio, σ_T/σ_L. If $\sigma_T/\sigma_L = 1$ then the transmission ratio is $T_{P2}/T_{P1} = 1$ independent of ϕ_T. The combined dependence of T_{P1} (Fig. 6) and $T_{P2}/$ T_{P1} on $I_{0L,1}$ allows the determination of both ϕ_T and σ_T. The best fit is obtained for $\phi_T = 1 - \phi_F \approx 0.999$ and $\sigma_T = 4.2 \times 10^{-17}$ cm². A high accuracy of σ_T and ϕ_T determination would be obtained, if σ_T were significantly different from σ_L. For C_{70} in toluene the singlet ground-state absorption cross-section, $\sigma_L = 3.5 \times 10^{-17}$ cm², and the T_1 triplet-state absorption cross-section, $\sigma_T = 4.2 \times 10^{-17}$ cm², are only slightly different. Therefore the accuracy of ϕ_T determination by T_{P1} and T_{P2}/T_{P1} measurement is moderate.

The second pump pulse transmission behaviour is simulated in Fig. 5. $T_{E,L2}$ depends on the T_1–T_l triplet absorption, σ_T, on the T_2–T_m triplet excited-state absorption, $\sigma_{ex,T}$, and on the triplet–triplet relaxation time, τ_T. Since σ_T has been already determined by probe pulse transmission measurements, the curves in Fig. 5 are calculated for various $\sigma_{ex,T}$ values ($\tau_T = 2$ ps, solid curves) and τ_T values ($\sigma_{ex,T} = 2.5 \times 10^{-17}$ cm², dashed curves) to study their dependences. For $\sigma_{ex,T}$ similar to σ_T, the second pump pulse transmission, $T_{E,L2}$, becomes practically independent of τ_T. Our numerical fit gives $\sigma_{ex,T} = (4.3 \pm 0.2) \times 10^{-17}$ cm², while σ_T has been determined to be $\sigma_T = (4.2 \pm 0.1) \times 10^{-17}$ cm². Therefore, determination of τ_T is not possible. In organic dyes typical values of τ_T are of the order of 0.5 to 3 ps [42,44].

6. Discussion

The determined parameters, σ_L, $\sigma_{ex,L}$, τ_{ex}, σ_T, $\sigma_{ex,T}$, and ϕ_T, of C_{70} in toluene at room temperature for $\lambda_L = 527$ nm are listed in Table 1 together with parameters reported in the literature.

Table 1
Spectroscopic parameters of C_{70} at room temperature

Parameter	Value	Comments
τ_{S_1} (ps)	110	[51]
	625	[9], undegassed
	627	[13], argon degassed benzene solution
	650	Used here
	660	[9], degassed
	670	[24]
	700	[27]
τ_P (μs)	0.710	[20], air saturated benzene solution
	0.730	[16], air saturated
	0.870	[18], air saturated benzene solution
	4–5	[18], argon-saturated
	41	[52], clusters in supersonic beam
	130	[16], degassed
	140	[21] in benzene
	53 000	[51], at 77 K in toluene/10% poly-(α-methylstyrene)
ϕ_F	0.00059	[14]
	0.0007	[9], in benzene
	0.00085	[9,16] and own measurement, used here
ϕ_T	0.76 ± 0.15	[21], in benzene
	0.9	[19]
	0.99 ± 0.02	[18]
	1 ± 0.15	[20], in benzene and hexane
	1 (≥ 0.85)	This work
$\tau_{FC,S}$ (ps)	0.5	Assumed [61], used here
$\tau_{FC,T}$ (ps)	0.5	Assumed, used here
τ_{ex} (fs)	240 ± 40	This work
τ_T (ps)	2	Assumed [42,44]
σ_L (cm^2)	3.2×10^{-17}	[21], in benzene
	3.5×10^{-17}	Own measurement, used here
k_{35} (s^{-1})	1.25×10^9	[15], in benzene
	1.54×10^9	$k_{53} = \phi_T \tau_{S_1}^{-1}$, used here
σ_T (cm^2)	3.6×10^{-17}	[23], in benzene
	3.8×10^{-17}	[21], in benzene
	3.9×10^{-17}	[20], in hexane
	$(4.2 \pm 0.1) \times 10^{-17}$	This work
	4.75×10^{-17}	[20], in benzene
$\sigma_{ex,L}$ (cm^2)	$(6.0 \pm 0.5) \times 10^{-17}$	This work
$\sigma_{ex,T}$ (cm^2)	$(4.3 \pm 0.2) \times 10^{-17}$	This work

Solvent toluene except stated otherwise.

The ratio of singlet excited-state absorption to singlet ground-state absorption is $\sigma_{ex,L}/\sigma_L \approx 1.7$. The S_1 state lifetime is $\tau_{S_1} \approx 650$ ps. For picosecond pulses (pulse duration, Δt_L, less than S_1-state lifetime, τ_{S_1}), C_{70} in toluene behaves as a reverse saturable absorber since $\sigma_{ex,L} > \sigma_L$. On a nanosecond time scale (pulse duration or time of observation longer than τ_{S_1}) the nonlinear transmission behaviour is determined by σ_T/σ_L. For C_{70} in toluene this absorption cross-section ratio is $\sigma_T/\sigma_L \approx 1.2$ and the reverse saturable absorption effect is rather weak.

Our double-pulse fluorescence measurements and probe pulse transmission measurements agree well with a quantum yield of triplet formation of $\phi_T \approx 1 - \phi_F$ ($\phi_F \approx 8.5 \times 10^{-4}$). Triplet quantum yields close to 100% have been reported by several groups (see Table 1). The S_1-state relaxation of C_{70} (as well as of C_{60} [4,17]) is dominated by intersystem-crossing. The rate of internal conversion is small compared to the rate of intersystem-crossing (because ϕ_T close to 1). The radiative relaxation time constant is long compared to the time constant of intersystem-crossing, τ_{isc} ($\tau_{isc} = k_{35}^{-1} = \phi_T \tau_{S_1} \approx 650$ ps; $\tau_{rad} \approx \tau_{S_1}/\phi_F \approx 760$ ns).

A higher-excited-state relaxation time of $\tau_{ex} = (240 \pm 40)$ fs has been determined for C_{70} in toluene. In organic dyes the higher-excited-state $S_n \rightarrow S_1$ singlet relaxation is generally fast in the 50 to 100 fs time range [62,63]. Only in the case of large energy gaps between S_2 and S_1 longer relaxation times are expected [64] and observed [65,66]. The symmetry of the C_{70} molecule and its weak S_0–S_1 absorption cross-section may be responsible for the moderate $S_n \rightarrow S_1$ relaxation time constant, τ_{ex}, of C_{70}.

7. Conclusions

The singlet and triplet absorption dynamics of C_{70} in toluene at room temperature has been studied with picosecond pulses at 527 nm. A double pump pulse induced fluorescence signal technique and a double pump pulse induced probe pulse transmission technique have been employed to determine the yield of triplet formation. Despite the fact of low fluorescence quantum yield and only slight difference between singlet ground-state and lowest-triplet absorption cross-sections, the quantum yield of triplet formation could be determined by both methods (fluorescence technique and absorption technique). The S_1–S_n excited-state absorption-cross-section, the S_n-state relaxation time, as well as the T_1–T_l and T_2–T_m absorption cross-sections have been determined.

The presented methods of double pump pulse induced fluorescence detection and double pump pulse induced probe pulse transmission measurement may be generally applied to the determination of quantum yields of triplet formation. The presented pump and probe pulse transmission analysis generally allows the extraction of excited-state absorption cross-section and excited-state relaxation parameters.

Acknowledgements

References

[1] H.W. Kroto, J.R. Heath, S.C. O'Brien, R.F. Carl, R.E. Smalley, Nature 318 (1985) 162.

[2] W. Krätschmer, L.D. Lamb, K. Fostiropoulos, D.R. Huffman, Nature 347 (1990) 354.

[3] M.S. Dresselhaus, G. Dresselhaus, P.C. Eklund, Science of Fullerenes and Carbon Nanotubes, Academic Press, San Diego, 1996.

[4] S. Leach, in: K. Prassides (Ed.), Physics and Chemistry of the Fullerenes, Kluwer Academic Publishers, Netherlands, 1994, pp. 117.

[5] S. Leach, M. Vervloet, A. Després, E. Bréheret, J.P. Hare, T.J. Dennis, H.W. Kroto, R. Taylor, D.R.M. Walton, Chem. Phys. 160 (1992) 451.

[6] H. Ajie, M.M. Alvarez, S.J. Anz, R.D. Beck, F. Diederich, K. Fostiropoulos, D.R. Huffman, W. Krätschmer, Y. Rubin, K.E. Schriver, D. Senskarma, R.L. Whetten, J. Phys. Chem. 94 (1990) 8630.

[7] J.P. Hare, H.W. Kroto, R. Taylor, Chem. Phys. Lett. 177 (1991) 394.

[8] J.B. Howard, J.T. McKinnon, Y. Makarousky, A.L. Lafleur, M.E. Johnson, Nature 352 (1991) 139.

[9] D. Kim, M. Lee, Y.D. Suh, S.K. Kim, J. Am. Chem. Soc. 114 (1992) 4429.

[10] Y.-P. Sun, P. Wang, N.B. Hamilton, J. Am. Chem. Soc. 115 (1993) 6378.

[11] R. Seshadri, C.N.R. Rao, H. Pal, T. Mukherjee, J.P. Mittal, Chem. Phys. Lett. 205 (1993) 395.

[12] Y.-P. Sun, B. Ma, G.E. Lawson, Chem. Phys. Lett. 233 (1995) 57.

[13] R.M. Williams, J.W. Verhoeven, Chem. Phys. Lett. 194 (1992) 446.

[14] Y.-P. Sun, C.R. Bunker, J. Phys. Chem. 97 (1993) 6770.

[15] A. Watanabe, O. Ito, M. Watanabe, H. Saito, M. Koishi, J. Phys. Chem. 100 (1996) 10518.

[16] J.W. Arbogast, C.S. Foote, J. Am. Chem. Soc. 113 (1991) 8886.

[17] L. Biczok, H. Linschitz, R.I. Walter, Chem. Phys. Lett. 195 (1992) 339.

[18] R.R. Hung, J.J. Grabowski, Chem. Phys. Lett. 192 (1992) 249.

[19] J.W. Arbogast, A.P. Darmanyan, C.S. Foote, Y. Rubin, F.N. Diederich, M.M. Alvarez, S.J. Anz, R.L. Whetten, J. Phys. Chem. 95 (1991) 11.

[20] D.K. Palit, A.V. Sapre, J.P. Mittal, C.N.R. Rao, Chem. Phys. Lett. 195 (1992) 1.

[21] R.V. Bensasson, T. Hill, C. Lambert, E.J. Land, S. Leach, T.G. Truscott, Chem. Phys. Lett. 206 (1993) 197.

[22] R.V. Bensasson, T. Hill, C. Lambert, E.J. Land, S. Leach, T.G. Truscott, Chem. Phys. Lett. 201 (1993) 326.

[23] N.M. Dimitrijević, P.V. Kamat, J. Phys. Chem. 96 (1992) 4811.

[24] K. Tanigaki, T.W. Ebbesen, S. Kuroshima, Chem. Phys. Lett. 185 (1991) 189.

[25] G. Sauvé, N.M. Dimitrijević, P.V. Kamat, J. Phys. Chem. 99 (1995) 1199.

[26] M. Gevaert, P.V. Kamat, J. Phys. Chem. 96 (1992) 9883.

[27] M. Lee, O.K. Song, J.C. Seo, D. Kim, Y.D. Su, S.M. Jin, S.K. Kim, Chem. Phys. Lett. 196 (1992) 325.

[28] F. Henari, J. Callaghan, H. Stiel, W. Blau, D.J. Cardin, Chem. Phys. Lett. 199 (1992) 144.

[29] C. Li, L. Zhang, R. Wang, Y. Song, Y. Wang, J. Opt. Soc. Am. B 11 (1994) 1356.

[30] M.P. Joshi, S.R. Mishra, H.S. Rawat, S.C. Mehendale, K.C. Rustagi, Appl. Phys. Lett. 62 (1993) 1763.

[31] B.L. Justus, Z.H. Kafafi, A.L. Huston, Opt. Lett. 18 (1993) 1603.

[32] A. Cost, L. Tutt, M.B. Klein, T.K. Dougherty, W.E. Elias, Opt. Lett. 18 (1993) 334.

[33] R.J. Sension, C.M. Phillips, A.Z. Szarka, W.J. Romanow, A.R. McGhie, J.P. McCauley Jr., A.B. Smith III, R.M. Hochstrasser, J. Phys. Chem. 95 (1991) 6075.

[34] D. McBranch, V. Klimov, L. Smilowitz, M. Grigorova, J.M. Robinson, A. Koskelo, B.R. Mattes, H. Wang, F. Wudl, SPIE 2854 (1996) 140.

[35] R.C. Issac, C.V. Bwidhu, S.S. Harilal, G.K. Varier, V.P.N. Nampoori, C.P.G. Vallabhan, Mod. Phys. Lett. B 10 (1996) 61.

[36] D.G. McClean, D.M. Brandelik, M.C. Brant, R.L. Sutherland, L. Frock, in: R. Crane, K. Lewis, E. Van Stryland, M. Khoshnevisan (Eds.), Materials for Optical Limiting, Symposium, Mater. Res. Soc., Pittsburgh, 1995, p. 293.

[37] N. Tang, H. Guan, J.P. Partanen, R.W. Hellwarth, SPIE 2143 (1994) 272.

[38] J.R. Heflin, W. Wang, C. Figura, R. Yordanov, SPIE 2530 (1995) 176.

[39] D. McBranch, L. Smilowitz, V. Klimov, A. Koskelo, J.M. Robinson, B.R. Mattes, J.C. Hummelen, F. Wudl, J.C. Withers, N.F. Borrelli, SPIE 2530 (1995) 196.

[40] L.W. Tutt, T.F. Boggess, Prog. Quant. Electron. 17 (1993) 299.

[41] Y. Song, X. Bao, F. Li, X. Yang, X. Zhang, R. Wang, C. Li, SPIE 2854 (1996) 230.

[42] S. Reindl, A. Penzkofer, Chem. Phys. 211 (1996) 431.

[43] S. Reindl, A. Penzkofer, Chem. Phys. 213 (1996) 429.

[44] A. Penzkofer, A. Beidoun, M. Daiber, J. Luminesc. 51 (1992) 297.

[45] W. Scheidler, A. Penzkofer, Opt. Commun. 80 (1990) 127.

[46] G. Grönninger, A. Penzkofer, Opt. Quant. Electron. 85 (1984) 473.

[47] D. von der Linde, O. Bernecker, A. Laubereau, Opt. Commun. 2 (1970) 215.

[48] V.D. Dimitrev, G.G. Gurzadyan, D.N. Nikogosyan, Handbook of Nonlinear Optical Crystals, Springer-Verlag, New York, 1991.

[49] Y.R. Shen, The Principles of Nonlinear Optics, Wiley, New York, 1984.

[50] A. Penzkofer, W. Bäumler, Opt. Quant. Electron. 23 (1991) 727.

[51] M.R. Wasielenski, M.P. O'Neil, K.R. Lykke, M.J. Pellin, D.M. Gruen, J. Am. Chem. Soc. 113 (1991) 2774.

[52] R.E. Haufler, L. Wang, L.P.F. Chibante, C. Jin, J. Conceicao, Y. Chai, R.E. Smalley, Chem. Phys. Lett. 179 (1991) 449.

[53] S. Reindl, A. Penzkofer, Chem. Phys. 230 (1998) 83.

[54] A. Samanta, J. Am. Chem. Soc. 113 (1991) 7427.

[55] V.V. Bryukhanov, B.F. Minaev, A.S. Kusenova, S.G. Karstina, J. Appl. Spectrosc. 56 (1992) 146.

[56] M.R.V. Sahyan, D.K. Sharma, Chem. Phys. Lett. 189 (1992) 571.

[57] H. Fukumura, K. Kikuchi, K. Koike, H. Kokubun, J. Photochem. Photobiol. A: Chem. 42 (1988) 283.

[58] W.G. McGimpsey, J.C. Scaiano, J. Am. Chem. Soc. 111 (1989) 399.

[59] H. Fukumura, K. Kikuchi, H. Kokubun, Chem. Phys. Lett. 92 (1992) 29.

[60] R.W. Redmond, I.E. Kochevar, M. Krieg, G. Smith, W.G. McGimpsey, J. Phys. Chem. A 101 (1997) 2773.

[61] A. Penzkofer, W. Falkenstein, W. Kaiser, Chem. Phys. Lett. 44 (1976) 82.

[62] C.V. Shank, E.P. Ippen, O. Teschke, Chem. Phys. Lett. 45 (1977) 291.

[63] F. Graf, A. Penzkofer, Opt. Quant. Electron. 17 (1985) 53.

[64] B.R. Henry, W. Siebrand, in: J.B. Birks (Ed.), Organic Molecular Photophysics, Vol. 1, Wiley, New York, 1973, p. 153.

[65] A. Maciejewski, A. Safarzadeh-Amiri, R.E. Verrall, R.P. Steer, Chem. Phys. 87 (1984) 295.

[66] M. Wittmann, A. Penzkofer, Appl. Phys. B 65 (1997) 761.